Cross-wire welding analyzed by experiments and simulations

Nielsen, C. V.; Zhang, W.; Bay, N.; Martins, P. A. F.

Published in:
Journal of Advanced Joining Processes

Link to article, DOI:
10.1016/j.jajp.2020.100039

Publication date:
2021

Document Version
Publisher's PDF, also known as Version of record

Journal of Advanced Joining Processes 3 (2021) 100039

Contents lists available at ScienceDirect

Journal of Advanced Joining Processes

journal homepage: www.elsevier.com/locate/jajp

Cross-wire welding analyzed by experiments and simulations

C.V. Nielsen [a,*], W. Zhang [b], N. Bay [a], P.A.F. Martins [c]

[a] Technical University of Denmark, Kgs. Lyngby, Denmark
[b] SWANTEC Software and Engineering ApS, Kgs. Lyngby, Denmark
[c] IDMEC, Instituto Superior Técnico, Universidade de Lisboa, Portugal

ARTICLE INFO

Keywords:
Cross-wire welding
Projection welding
Resistance welding machines

ABSTRACT

Resistance welding of crossed wires, e.g. used in the electronics industry or in fabrication of wire meshes, is analyzed by both experiments and numerical modeling using an electro-thermo-mechanical finite element formulation. Welding machine characteristics are discussed and the necessary requirements to the type of welding machine are concluded. Cross-wire welding of stainless steel, structural steel and aluminum are presented, and differences in the welding process and flash formation are discussed. It is shown that the joints are primarily due to solid-state bonding and local melting. The simulations compare well to the experiments at low weld settings, while remaining challenges for simulation of high weld settings are identified in terms of requirements to the mesh and detailed description of the machine follow up of the electrode force and movement.

1. Introduction

Cross-wire welding is among the most common non-automotive applications of resistance welding, see e.g. Scotchmer (2007). The primary use of cross-wire welding is in the electronic industry and in the fabrication of wire meshes. In electronics, wires are welded to each other in light bulbs as presented by Goodman (1950), who also discusses the loads that the joints will encounter during the life of the light bulb together with eventual failure modes. Knowlson (1967) gives other examples of cross-wire welding in electronics; namely welding of a variety of components, such as resistors, capacitors, diodes and transistors, into small closely packed devices. Wire meshes are used in various products in kitchen wear, shopping carts and for reinforcing concrete structures. Resistance welding poses an alternative to woven structures of wire meshes that are also commonly used. In large scale production of wire meshes, entire rows of cross-wire welds are performed simultaneous as e.g. presented by Jordan (1964) and Bushell (1951).

Experimental studies of cross-wire welding have mostly focused on optimizing weld schedules with respect to setdown and weld strength as e.g. Jones (1948) Wängsjö and Palmqvist (1958). Fukumoto et al. (2008) studied cross-wire welding of micro wires and the resulting microstructures and strength.

Numerical modeling of cross-wire welding is rarely seen in literature. One contribution was given by Scotchmer (2007), who presented 2D numerical simulations by SORPAS® with good comparison to experimental cross-wire welds. This has required trial-and-error calibration of the third dimension in terms of the thickness of the elements varying through the cross-section. A compromise must have been necessary for obtaining enough mechanical stiffness by thick elements, while having elements thin enough to concentrate and generate heat. Later, Mikno (2018) and Iatcheva et al. (2018) applied 3D simulation to study welds with low setdown.

The present work discusses welding machine characteristics for cross-wire welding and present experimental results from welding of wires of stainless steel, structural steel and aluminum. The above mentioned applications of cross-wire welding involve various wire diameters and materials. Wire diameters of 10 mm are chosen for the present experiments. This diameter lies within the range of diameters used for wire meshes used in reinforcing concrete. The different behaviors and challenges for each of the materials and their surface conditions are discussed. The bonding mechanisms for each material are also presented. Finally, 3D numerical modeling, using SORPAS®, of cross-wire welding is presented and compared to the experimental results for low weld settings, while challenges at high weld settings are discussed.

2. Experimental setup and selection of welding machine

2.1. Cross-wire welding setup

Cross-wire welding of Ø10 mm × 100 mm wires is performed in the setup shown in Fig. 1 between Ø30 mm flat C0-type electrodes. The wires are aligned in the guiding system (Fig. 1b) such that they are perpendicular to each other with the intersection point centered relative to the electrodes. The wires are free to move vertically, so that the guides do not provide any stiffness disturbing the welding process. The lower wire rests on the lower electrode, while the upper wire is balancing on top of the lower wire by means of e.g. a piece of paper squeezed in between the

* Corresponding author.
E-mail address: cvni@mek.dtu.dk (C.V. Nielsen).

https://doi.org/10.1016/j.jajp.2020.100039
Received 17 October 2020; Received in revised form 4 December 2020; Accepted 4 December 2020

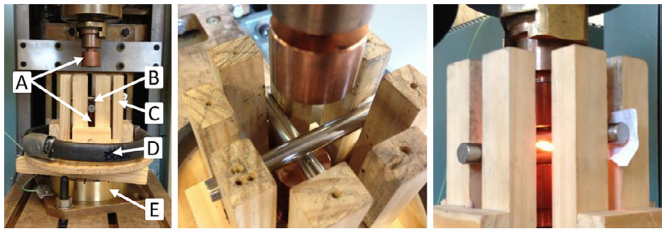

Fig. 1. Resistance projection welding of two crossed wires. (a) Setup between two flat C0-type electrodes A. The two crossed wires B are aligned perpendicular to each other and centered between the electrodes by the guidance C holding a Rogowski coil D for measuring the welding current. Below the lower electrode is placed a force transducer E for measuring the welding force. (b) Close-up showing the perpendicular aligned wires resting on the lower electrode in the guidance. (c) Photograph of the cross-wire welding.

wire and the guiding system (Fig. 1c), which is not adding any relevant vertical constraint during the welding process. The horizontal alignment is naturally solved as soon as the upper electrode presses towards the wires. During welding (as photographed in Fig. 1c), the electrode force and the welding current are measured by a load transducer and a Rogowski coil positioned as shown in Fig. 1a.

Wires of three materials are considered. These are aluminum AA6060-T6, structural steel S235JR+AR and stainless steel AISI 316L. Flow stress curves as function of temperature and strain rate are obtained on a Gleeble 1500 system (see Nielsen 2012) and presented in Fig. 2. Note that the structural steel S235JR+AR deviates from the typical softening with temperature due to blue brittleness around 400°C. Electrical and thermal material data are available in the material database of SORPAS® (2020).

One of the evaluation parameters for cross-wire welding is the setdown S as defined in Resistance Welding Manufacturers' Association (2003),

$$S = \frac{A - B}{A} \tag{1}$$

where A is the initial wire diameter and B is the final height of the joint subtracted one diameter A; see Fig. 3. The setdown is a direct measure of the compression and for a given force level an indirect measure of the heat input. It also relates to the weld strength to some degree.

2.2. Selection of welding machine

Two welding machines have been evaluated. The major differences between the two machines are the source of applied weld force and type of welding current. One is a 8105 Tecna 250 kVA with a TE 180 control unit (hereafter called Tecna). The other is an Expert 170kVA with Harms & Wende HWI 2000 control unit (hereafter called Expert).

The Tecna has a pneumatic force system and supplies AC welding current, while the Expert has a hydraulic force system with additional disc springs to stabilize the force and supply a constant force during eventual collapse of material due to softening. The Expert supplies a middle frequency, 1 kHz, welding current, practically acting as a DC current.

Preliminary welding tests were made on both of the machines showing significant differences in the behavior for projection welding. The most severe differences were observed when welding the wires of aluminum, which has relatively high thermal and electrical conductance, resulting in modest heat generation and quick heat conduction away from the weld zone. Thus, welding of aluminum generally requires short welding time and high welding current, resulting in a narrow process window because the minimum current required to produce a weld is already close to the splash limit.

It was impossible to get sufficient setdown and strength in cross-wire welding of aluminum in the Tecna. The typical problem observed when welding the aluminum wires by the Tecna is the sudden jump from low setdown to heavy expulsion due to a slight increase in welding current as shown by Fig. 4a and 4b. An example of a weld obtained by the Expert is given in Fig. 4c, where the wires were glass blasted for increased consistency in the experiments later conducted in the Expert.

The major reason for this sudden change in welding behavior in the Tecna is attributed to the pneumatic force system, which cannot follow up the force and movement when the material softens. The contact area is therefore not properly developed and the high current produces very high temperatures locally resulting in heavy splash on the free surfaces. Another issue relevant to consider in aluminum welding is the type of supplied welding current. When using AC current, the time in-between the peaks with sufficient current will act as cooling time because the low current is not sufficient to heat or even to maintain the temperature in the aluminum near the weld region because of the high thermal conductivity of aluminum. The periods of time without current due to conduction angles less than 100% act in the same way, which requires higher current and hence higher peaks with higher risk of splash.

Batten (1958) reported similar experiences with a pneumatic force control and improved the follow-up of the electrode movement when the cross-wire collapses by a sudden release of the pressure on one side of the piston. This allowed reasonable welding but was less controllable. Batten (1958) also reported splash in some cases and proved by use of a photo-cell that it always happened near the current peaks in agreement with the above discussion.

Welding on the Expert on the other hand gives the possibility of joining aluminum cross-wires with stable development of setdown as function of welding current. The major benefit gained with the Expert is the hydraulic force control with inserted disc springs between the piston and the weld electrode. The disc springs are designed to follow up the movement of the electrode while keeping the force constant. When the material collapses in projection welding, the load on the springs decreases, which results in expansion that will push the electrode down to follow the specimens being welded. In addition, the middle frequency, DC-like, welding current avoids the above concerns of the current peaks.

The cross-wire welding of aluminum requires the use of the Expert welding machine. The stainless steel can be welded easily on both of the machines. On the contrary to the expectation, it appears that the structural steel is easier welded on the Tecna. The as-received structural steel was welded without problems on the Tecna, while resulting in splash already at low current settings on the Expert. This was proven to be related to the surfaces conditions. After removing the black surface by grinding, the structural steel was also easily welded on the Expert. One explanation could be that when using the AC current in the Tecna, the surface layer is softened and squeezed out during the initial stage of the first quarter cycle of the current before the full current is supplied, since Thornton et al. (1996) report that the major change in the electrical contact resistivity happens within the first quarter cycle.

To conclude the discussion of the differences between the two welding machines, it is noted that all following welds were made by the Expert welding machine.

2.3. Surface preparation of the wires

Due to the above discussion, the structural steel wires were ground before welding. The aluminum wires were glass blasted at least three hours before welding in order to obtain consistent results. All aluminum wires were welded in the same day as they were glass blasted. The glass blasting removes the existing oxide layer and a new even layer can develop before welding. All wires were cleaned with benzine before welding.

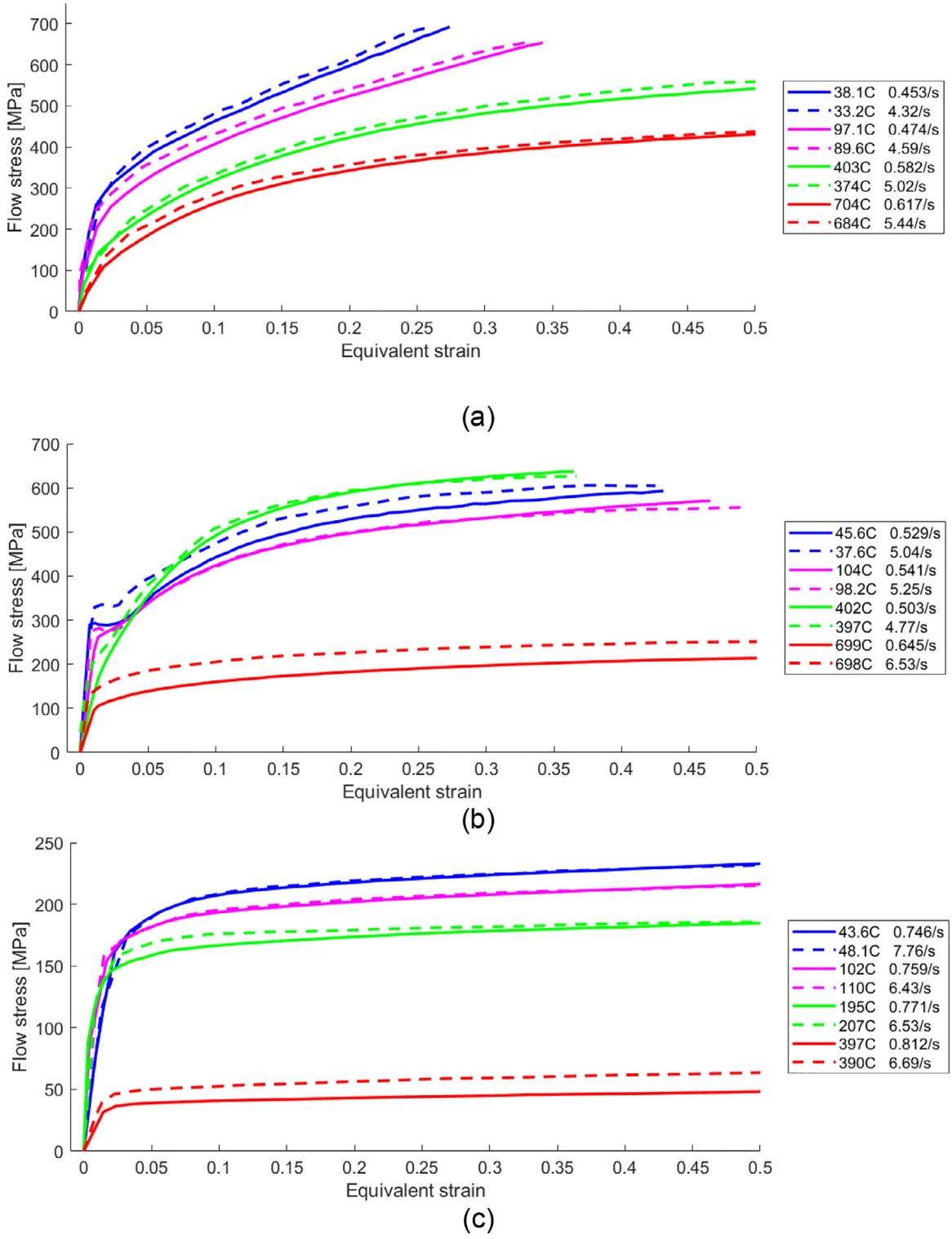

Fig. 2. Flow stress curves as function of temperature and strain rate for (a) AISI 316L, (b) Steel 235 and (c) AA6060-T6.

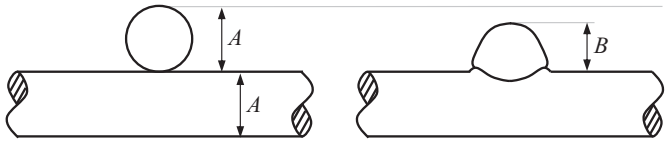

Fig. 3. Parameters *A* and *B* for definition of setdown.

2.4. Welding parameters

An example of measured welding current and force from welding on the Expert is shown in Fig. 5. The example originates from cross-wire welding of stainless steel wires through 600 ms weld time with specified weld current 12 kA under electrode force 10 kN. The measured current (Fig. 5a) oscillates around a mean value of 11.5 kA. The force is stable

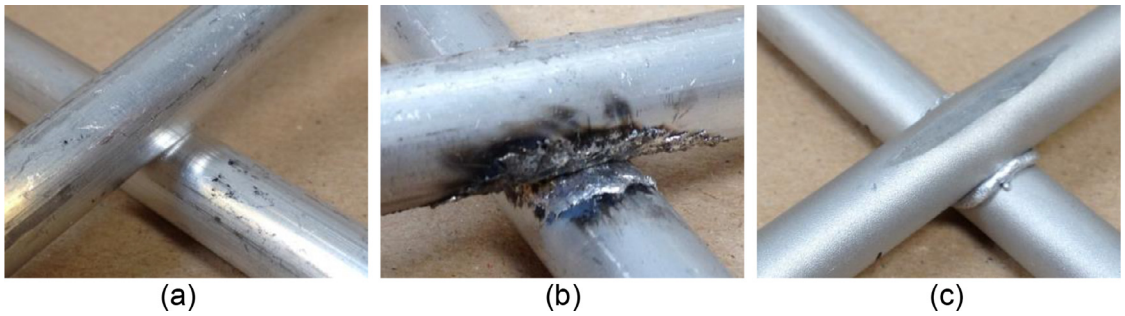

Fig. 4. Examples of cross-wire welded aluminum. (a) Low weld setting in Tecna. (b) Slight increase of current in Tecna with resulting heavy expulsion. (c) High weld setting and glass blasted surfaces in Expert.

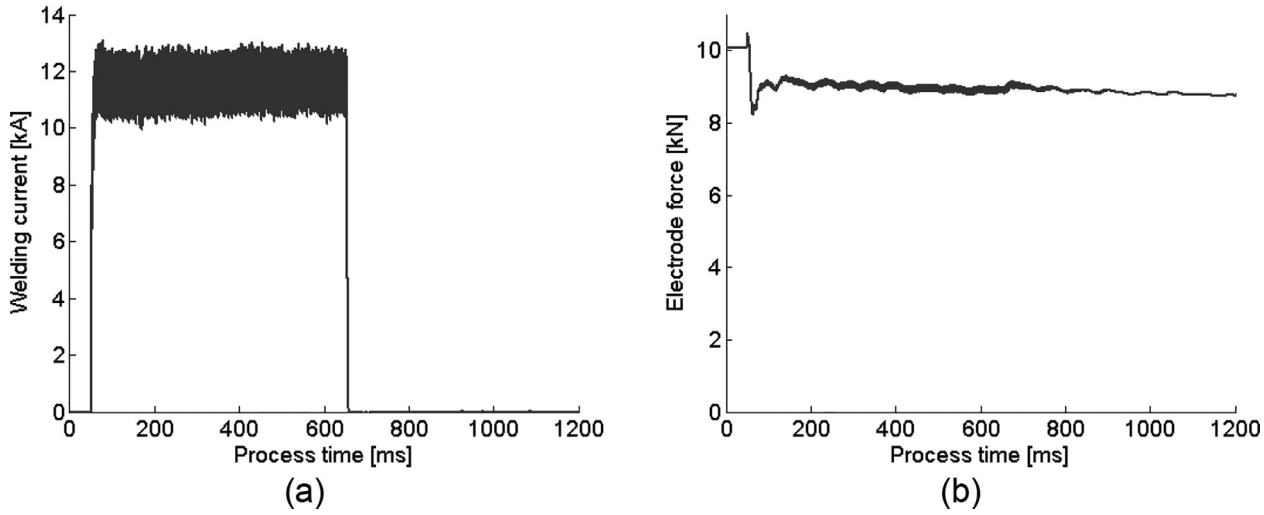

Fig. 5. Example of measured welding current (a) and force (b) as function of process time.

at 10.1 kN before applying the current. When the current is applied, the force is shortly increased to around 10.5 kN due to thermal expansion, while softening of the material is giving rise to the immediate drop in force level to around 8.4 kN. The force stabilizes hereafter at 9.0 kN for the remaining process time. The average electrode force during the welding time is 9.0 kN. These process curves are representative for the welds presented in the following, where the process parameters are presented by the current setting (here 12 kA), the weld time (here 600 ms) and the average measured electrode force (here 9.0 kN).

3. Experimental results

3.1. Setdown for all three materials

The setdown for all the cross-wire welding experiments conducted on the Expert are shown in Fig. 6. The stainless steel AISI 316L and structural steel S235JR+AR are welded with the same settings of electrode force and weld time and presented in Fig. 6a as a function of the current. The aluminum, AA6060-T6, is welded at lower electrode force and shorter weld time because of the lower strength and the high electrical and thermal conductance properties of aluminum, which at the same time give rise to a higher current level to facilitate welding. Fig. 6b presents the setdown as function of current for the aluminum cross-wire welds. The figure also includes the results obtained with the two steels. Despite the different force levels and weld times, the comparison is relevant for showing the differences in applied currents. The comparison also shows that similar setdowns are obtainable in the Expert welding machine.

The stainless steel experiences a larger setdown than the structural steel welded under similar conditions. This is mainly because of larger heat generation due to larger electrical resistivity and poorer heat conduction in the stainless steel.

The figures include indication of splash by the square markers. It is noted that the splash behavior and the resulting appearance is different from splash in spot welding. In spot welding the weld nugget is enclosed between the sheets and splash is a result of escape of an amount of molten material between the sheets facilitated by the pressure in the enclosed molten volume great enough to penetrate the closing area of the sheets. It is visible by the related flash when it occurs, and it is visible afterwards as the escaped material typically solidifies on the sheets outside the spot weld. In cross wire welding, splash typically occurs from the material that is already squeezed out (see material piled up around the weld in Fig. 4c). As a result of this, the splash occurs from a volume under much less pressure and the appearance is a small drop jumping from the free surface. This may produce a small cone point from the place it left, but depending on the remaining process, it may also even out. Furthermore, the drop leaving the weld zone has large possibility of hitting elsewhere than the wires. Summing up, it is more difficult to record all splashes and it is less damaging for the weld when it occurs.

Three points on each curve in Fig. 6 are selected for further analysis with capital letters A-I for identification. Each of these points includes five repetitions, which practically coincide. One of the five repetitions for each point is selected for further analysis and have details presented

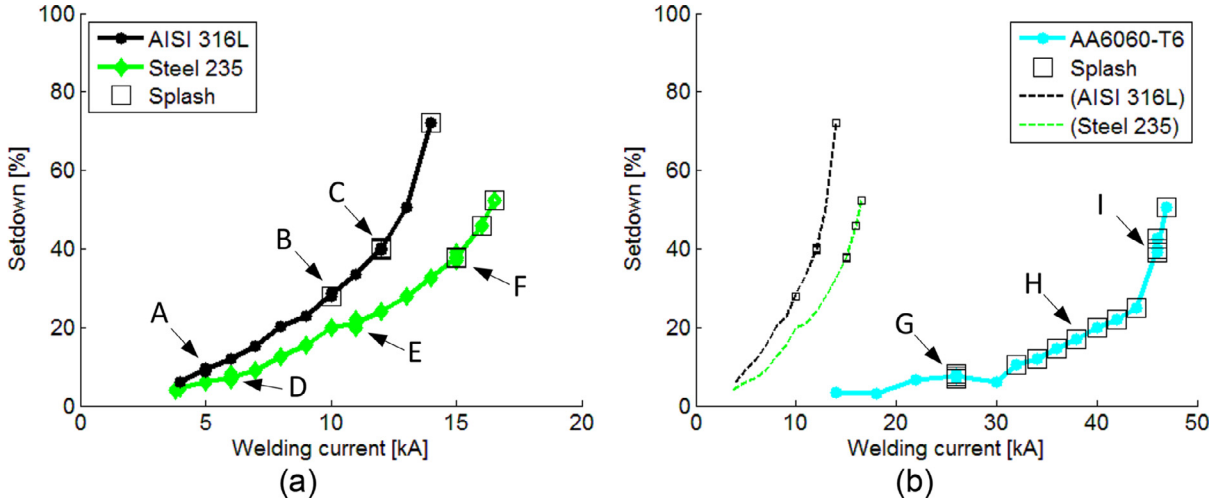

Fig. 6. Setdown as function of current for (a) stainless steel AISI 316L (force: 8.9-9.4 kN) and structural steel S235JR+AR (force: 8.5–9.8 kN) with weld time 600 ms, and (c) aluminum AA6060-T6 with force 4.2-5.5 kN and welding time 140 ms, where also the two steels are included for comparison of current level, though with different electrode force and weld time. Three points on each curve (marked A-I) include five repetitions and are selected for further analysis.

Table 1
Welding parameters, setdown and list of related figures for the selected welds A-I.

Wire material	Weld label	Weld current [kA]	Electrode force [kN]	Weld time [ms]	Resulting setdown [%]	Related figures
AISI	A	5	9.1	600	9.5	6a,7a,7d,14
316L	B	10	9.0		29	6a,7b,7f
	C	12	9.0		40	6a,7c,7e,7g
Steel	D	6	8.8	600	7.5	6a,8a,8d,8e,15
235	E	11	8.7		20	6a,8b,8f,8g
	F	15	8.6		38	6a,8c
AA6060-	G	26	5.2	140	7.0	6b,10a,10d,16
T6	H	38	4.8		17	6b,10b,10e,11,12
	I	46	4.4		43	6b,10c,10f,10g

in Table 1. Cross-sectional analysis of the selected welds are presented in the following.

3.2. Cross-sections of stainless steel AISI 316L wires

The three selected stainless steel welds, A-C, are shown in Fig. 7a-c. The development of the weld can be extracted from the overall geometry resulting from different current levels. The wires initially deform such that material is starting to flow out from the contact interface (Fig. 7a). When the generated heat is higher, the material softens with larger amount of material squeezed out between the two wires (Fig. 7b,c).

The type of material flow changes with heat input. At low heat input, the magnified cross-section in Fig. 7d shows that the deformed material near the interface kept substantial strength and stayed in the solid phase because of the sharp edges remaining. This is seen in the figure despite the many scratches, which originate from particles falling off from the material during grinding. The particles, mainly originating from the left side in the figure, scratch the cross-section during further grinding. This has happened in many of the cross-sections presented in the following, though to a lesser extent than in Fig. 7d. When the material is softened more due to larger heat input (Fig. 7b,c), the flow changes to produce more rounded geometries. The magnifications in Fig. 7e,g show a resulting mushroom shaped squeeze-out of material. The magnifications show that this flow originates from a narrow opening between the wires, which has happened in a mushy or melted state of the material.

The microstructure suggests that there has been no other melting, and hence there is no weld nugget and the welding is not characterized by fusion. It can be compared to friction welding where the joining is facilitated by elevated temperatures (without melting) and high pressure. The observation and corresponding conclusion is supported by Pan and Watt (1995), who also characterize cross-wire welding by having no or little melting, but rather sinking of the two wires into each others' softened zones. They further support the link to friction welding. Fukumoto et al. (2006) consider cross-wire welding to be a solid-phase joining process because any liquid phase is expelled together with oxide layers and will appear outside the joining area. Khan et al. (2009) examined cross-wire welding of stainless steel and supported the process description by Fukumoto et al. (2006). Khan et al. (2009) investigated the transition between solid state bonding and fusion welding concluding that fusion welding needs lower electrode force and/or higher weld current in agreement with the nature of heat development.

3.3. Cross-sections of structural steel S235JR+AR wires

The cross-sections, D-F, for the structural steel welds are shown in Fig. 8. This steel type shows clear phase and structure changes in the microstructure. The heat affected zone (most clear in Fig. 8g) consists of two regions. The central volume has been above the austenitization temperature and the surrounding heat affected zone has been in the transition zone. The zone around the interface seems to have been kept below the melting temperature during all three welds.

The magnifications at low heat input (Fig. 8d,e) show a clear identification of the original interface. The material is only joined by local welds across the interface. At larger heat input levels (Fig. 8f,g), an interesting difference appears when comparing to the stainless steel welds. The material is squeezed out to produce a sharp edge and in the case with more setdown (Fig. 8g) producing two sharp edges because the material from each side curls to keep the circumferential tension low

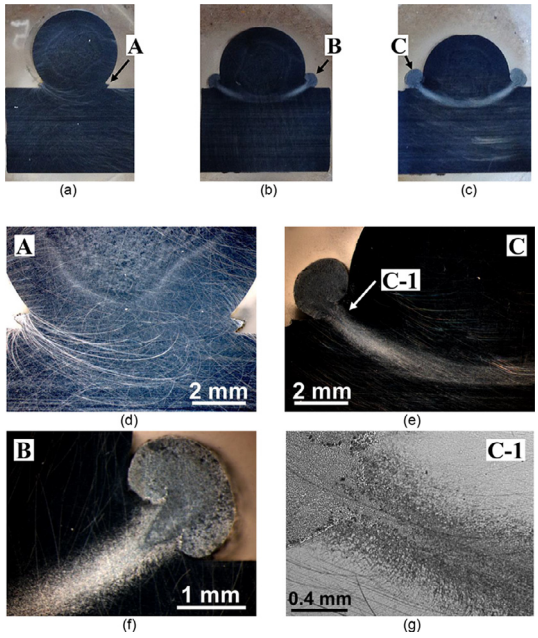

Fig. 7. Cross-sections of selected stainless steel AISI 316L cross wire welds. (a) Weld A with 9.5% setdown. (b) Weld B with 29% setdown. (c) Weld C with 40% setdown. (d–f) Magnifications with positions indicated in (a–c). (g) Further magnification of position marked in (e).

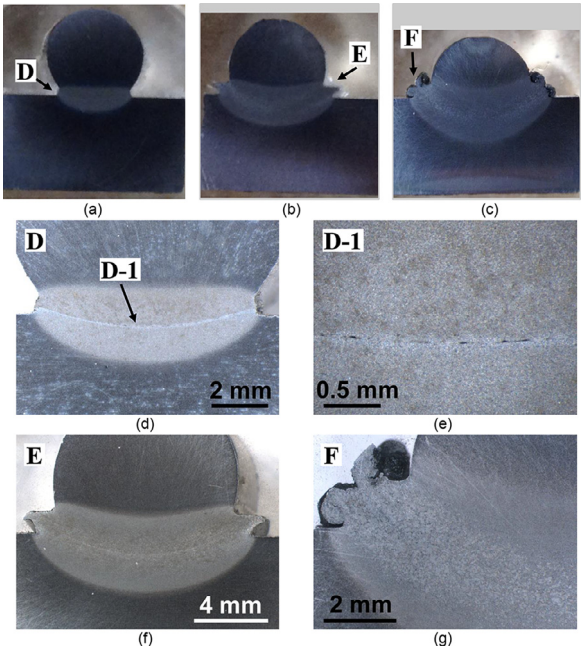

Fig. 8. Cross-sections of selected structural steel S235JR+AR cross-wire welds. (a) Weld D with 7.5% setdown. (b) Weld E with 20% setdown. (c) Weld F with 38% setdown. (d,f,g) Magnifications with positions indicated in (a–c). (e) Further magnification of position marked in (d).

by minimizing the radius. Since the material curls both ways, it has not been sufficiently joined before being squeezed out.

The explanation of the differences between the two steel types in the shape of the squeezed out material cannot be explained by the stainless steel being liquid and the structural steel being solid when forming the expelled shape, as it may look like at first. Returning to the comparison to friction welding, Fig. 9 shows a photograph of a friction weld that joins a mild steel and a stainless steel, where none of the materials were

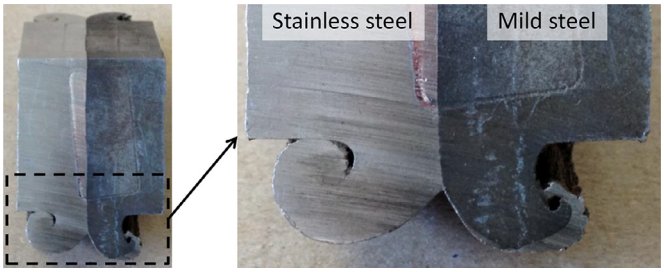

Fig. 9. Example of friction welded mild steel to stainless steel. The geometries of the formed flashes of the two materials are comparable to the shape of the material squeezed out during cross-wire welding.

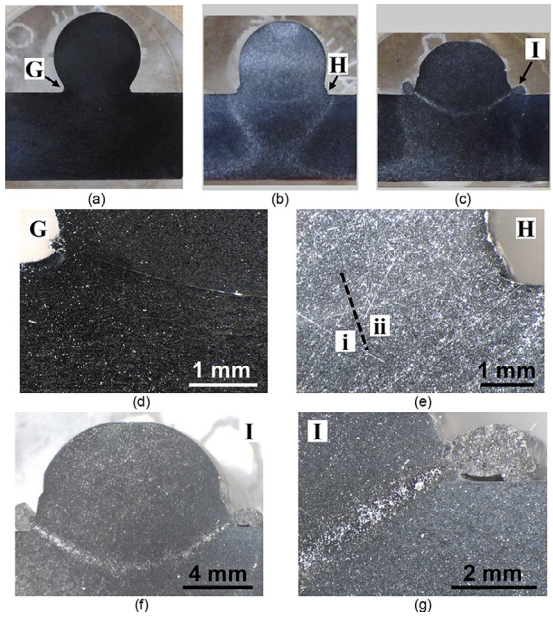

Fig. 10. Cross-sections of selected aluminum AA6060-T6 cross-wire welds. (a) Weld G with 7.0% setdown. (b) Weld H with 17% setdown. (c) Weld I with 43% setdown. (d–g) Magnifications with positions marked in (a–c).

melted. This joint shows the same shape of the produced flashes in the two materials as appear in the material squeezed out during cross wire welding.

3.4. Cross-sections of aluminum AA6060-T6 wires

Finally, the aluminum cross-wire welds, G-I, are shown in Fig. 10. The tendency of squeezing out material seems less than in the above cases including steel wires. From a heat generation point of view, this is explained by the fast heat conduction that softens the material more evenly than in the cases with stainless steel and structural steel. When the material is overall softer, it experiences more global deformation when enlarging the area supporting the electrode force. It is supported by an explanation from the electrode force itself, which has been selected too high for optimal welding. The larger force results in a larger initial contact area with lower heat concentration as a consequence.

This is supported by the appearance of the interface between the joined wires. At low heat input and setdown (Fig. 10a,d), a clear interface is observed between the two wires. The largest setdown (Fig. 10c,f,g) associated with high heat input has a more mature bond, while the medium setdown and heat input (Fig. 10b,e) lies somewhere in between. Weld H has the central part of the interface intact and only a solid joint on the outer ring. This is to some extent visible from Fig. 10b and by the regions i (center) and ii (outer ring) in Fig. 10e. It is shown

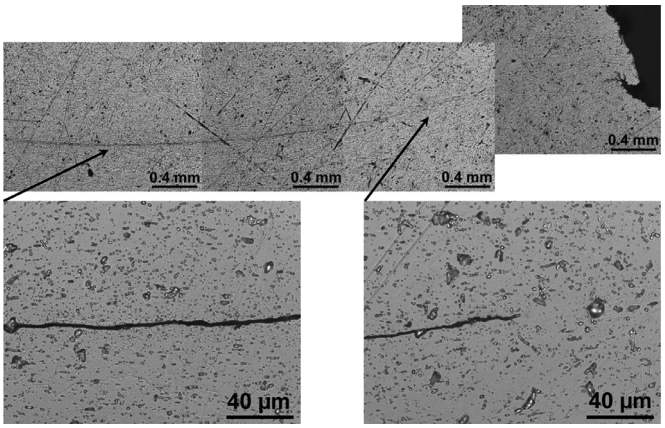

Fig. 11. Magnified cross-section of aluminum weld H around the interface in a similar view as Fig. 10e. The upper row of four photos are assembled to reproduce half of the interface and the two lower photographs are further magnifications.

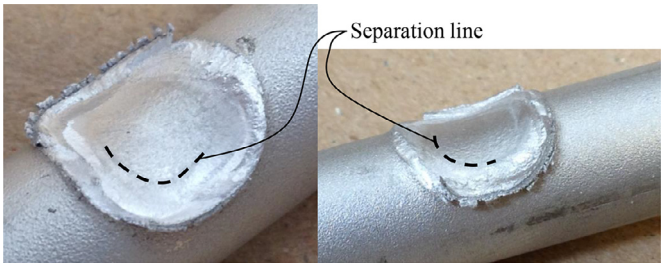

Fig. 12. Separated aluminum wires of weld H corresponding to Fig. 10b,e and Fig. 11 (another of the five repetitions). The partially indicated separation line shows the transition from no bonding in the center to bonding on the outside.

with further magnifications in Fig. 11, where the original interface is clear in the center of the weld while the outer ring is joining the two wires. Another weld from point H (i.e. another of the five repetitions) is shown in Fig. 12 after separation of the two wires. This figure shows the central area of the former weld to have a blank surface without signs of fracture. The surface even stays close to the original glass blasted condition. The joint has only been facilitated by the welded outer region, which shows signs of fracture and partial fracture.

Improvement of the aluminum welds would require lower electrode force to allow heat development before increasing the contact area too much.

4. Numerical model

4.1. Initial mesh

This section presents 3D numerical simulations of cross-wire welding and comparisons to the above experiments. The finite element mesh utilized for the simulations is shown in Fig. 13. One quarter of the physical geometry is simulated by utilizing the two vertical symmetry planes that go along the wires. The mesh consists of approximately 8000 hexahedral elements with mesh density increased around the contact between the two wires, where the weld takes place. The governing equations for the finite element simulations are extensively described elsewhere (Nielsen et al., 2013, Nielsen et al., 2015, Nielsen et al., 2015), and further details of the commercial software is available at (SORPAS® 2020).

4.2. Comparisons for low weld settings

Comparisons of simulations and experiments of the cross-wire welds carried out at low weld settings are shown by Fig. 14–16. For the stainless steel, this corresponds to weld A among the experiments; see Fig. 6a for identification of the weld and Fig. 7a for the experimental cross-section. The weld settings include 5 kA weld current applied during 600 ms under an applied electrode force of approximately 10 kN.

Fig. 14 shows the comparison for this case in terms of the resulting geometry in the cross-section. The simulation shows the process peak temperature reached until the end of the weld time with an overall peak temperature 1224 ˚C, which is below the melting point (1400 ˚C for AISI 316L) as anticipated in the discussion of the experiment. The overall deformation is evaluated by the setdown, which for the experiment is 9.5%. The simulation shows 14% setdown (and 15% setdown after the hold time), corresponding to a final height difference of 0.45 mm (and 0.55 mm after the hold time) out of 20 mm total height before welding.

Besides the larger setdown obtained in the simulation, a noticeable difference is that the experiment shows initiation of flash formed between the two wires and the simulation does not catch this. Part of the explanation can (as always with simulations) be attributed to uncertainties in material properties, but the mesh itself is considered to play a bigger role in the specific example because of being too coarse to reproduce the actual deformation. With too few elements that can only reproduce the geometry changes trilinearly, it is not possible to simulate the local softening and deformation associated with the initiated flash. Another issue that complicates the simulation of the local deformation is that the mesh does not conform to the formed contact area and the flashing (see ring markers in Fig. 14), and hence even more elements would be required. The lacking flash formation in the simulation causes the simulated contact area to remain smaller than in the experiment during the flash formation. This results in more heat generation and material softening over a larger volume, leading to bulk deformation and finally larger setdown than in the experiment.

Mesh refinement and remeshing are important for modeling of such local deformation. As regards remeshing, it is important that the remeshing is capable of concentrating elements around the local details in the weld zone. Resmeshing during simulation of projection welding is done in (Nielsen et al., 2013), but without respecting mesh refinements. Challenges in relation to modeling of the flash formation are described further in Section 4.3.

A similar comparison is shown in Fig. 15 for the structural steel, where better agreement between simulation and experiment is obtained because this weld does not include initiation of flash formation. The actual weld considered is the above weld D, which can be identified in Fig. 6a and found by cross-sections in Fig. 8a and 8d. The weld settings include 6 kA weld current applied during 600 ms under an applied electrode force of approximately 10 kN. Again the overall deformation is evaluated by setdown, which for the experiment is 7.5%. The simulation shows 9.4% setdown (and 9.5% setdown after the hold time), corresponding to a final height difference of 0.19 mm (and 0.20 mm after the hold time) out of 20 mm total height before welding.

Fig. 15a shows the overall comparison of simulated geometry to the experiment by its cross-section. It also includes comparison of the temperatures in terms of iso-thermal contour lines at 700 ˚C and 900 ˚C which are mirrored on to the experiment, where the microstructural changes reveal the temperatures obtained during the actual welding. Fig. 15b shows the comparison in a magnified view, where the 900 ˚C iso-thermal line, which roughly equals the austenitization temperature, practically coincides with the border line between two different microstructures. The volume within the lines is transformed into austenite during welding and is formed into a fine recrystallized grain structure upon cooling. This confirms that both the deformation and heat generation are simulated with high accuracy in this example. It is further justified by a simulated maximum temperature of 1221 ˚C, in agreement with the experiment showing no sign of melting (assumed 1560 ˚C for S235JR+AR).

Finally, Fig. 16 shows the comparison with aluminum wires as the above weld G, which is identified in Fig. 6b and Fig 10a. The weld set-

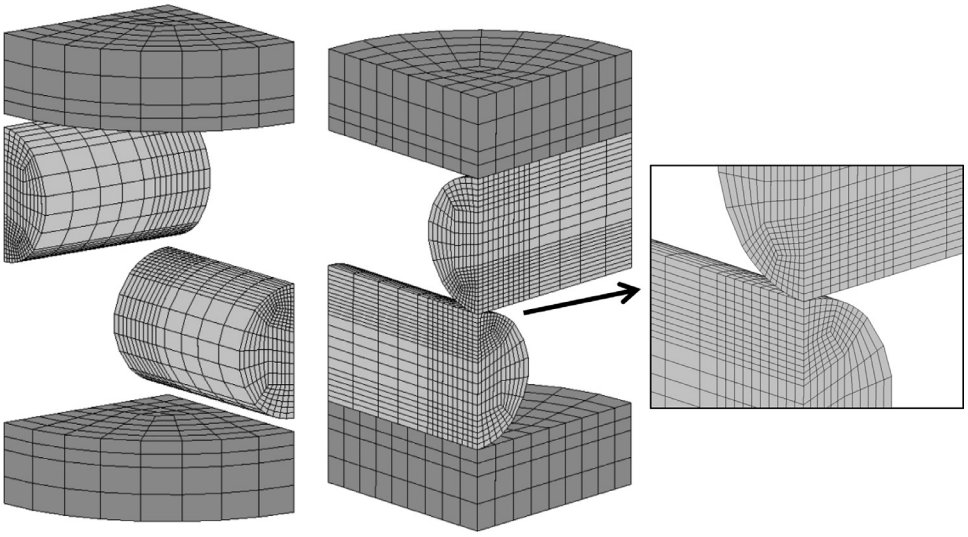

Fig. 13. Finite element mesh for simulation of cross-wire welding by application of two symmetry planes. The right figures show the local mesh refinement and an example of the formed contact between the two wires.

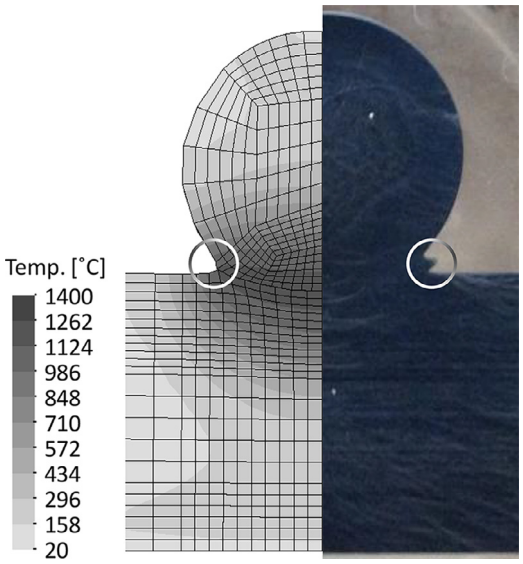

Fig. 14. Comparison of simulation and experiment for weld A (Fig. 6a and Fig. 7a) consisting of two stainless steel rods welded at low weld settings. The simulation shows the process peak temperature reached at the end of the welding time. Ring markers identify the location of the flash.

tings include 26 kA weld current applied during 140 ms under an applied electrode force of approximately 5.5 kN. The setdown in the experiment is 7.0%, while the simulated setdown is 13% (still 13% setdown after the hold time), corresponding to a final height difference of 0.60 mm out of 20 mm total height before welding. The final geometry of the experiment does not show any flash formation, so the explanation for the difference is not the same as for the stainless steel cross-wire in Fig. 14. The larger setdown in the simulation of the aluminum cross-wire is rather attributed to the indentation in the bulk material, which is visible in the simulation as an amount of material piling up outside the contact area. The reason can either be overestimation of the heat generation, too soft material properties in the simulation or a combination of both.

It is likely that the mechanical material properties are not accurate since also the pure mechanical contact experiments with the same materials presented in (Nielsen et al., 2011) showed inaccuracies when simulating aluminum. The glass blasting may further influence the properties and the formation of contact area.

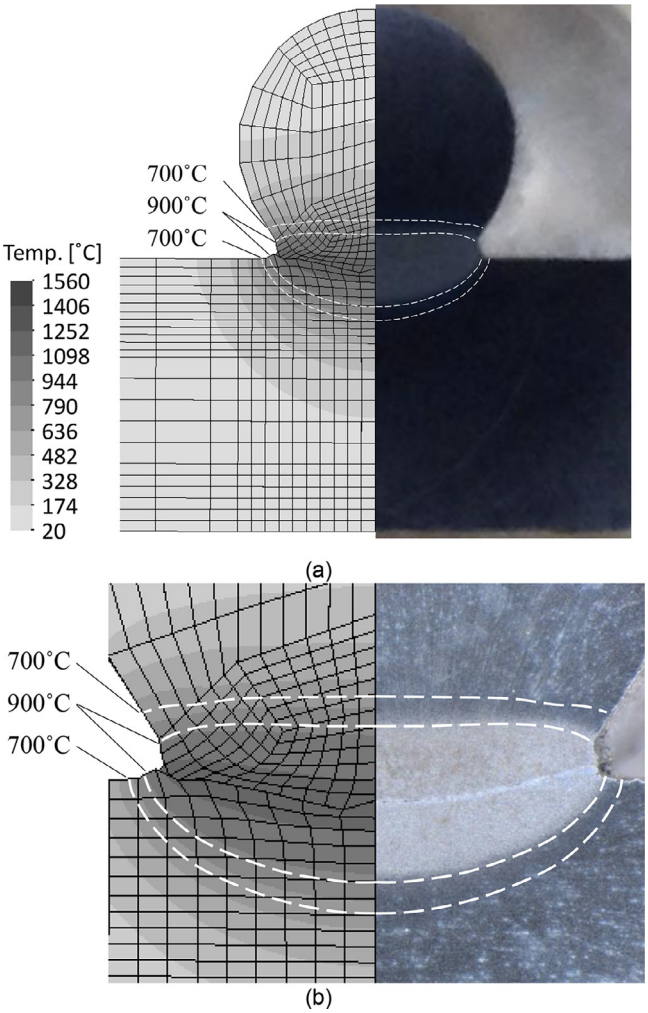

Fig. 15. Comparison of simulation and experiment for weld D (Fig. 6a, Fig. 8a for subfigure (a) and Fig. 8d for subfigure (b)) consisting of two structural steel rods welded at low weld settings. The simulation shows the process peak temperature reached at the end of the welding time together with corresponding, selected iso-thermal lines mirrored on top of the experiment.

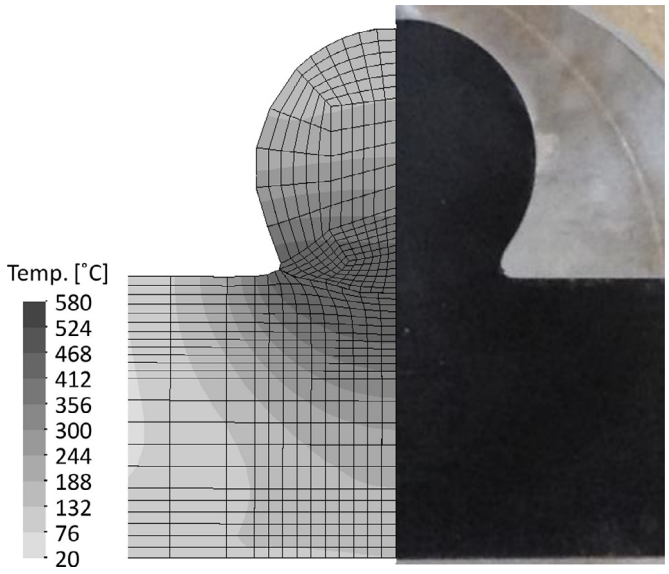

Fig. 16. Comparison of simulation and experiment for weld G (Fig. 6b and Fig. 10a) consisting of two aluminum rods welded at low weld settings. The simulation shows the process peak temperature reached at the end of the welding time.

4.3. Challenges in simulation of high weld settings

When it comes to cross-wire welding with high weld settings, the simulations cannot predict the actual heat generation and the final setdown. When examining the cross-sections corresponding to medium or high weld settings in Fig. 7, 8 and 10, it appears that material is squeezed out between the two wires because of the high degree of local softening and eventual melting. The local type of deformation is suited for a typical simulation by itself and thus not possible to simulate by the few elements available for the local details. Hence, the discussion given in relation to the initiation of flash formation for the stainless steel welding under low weld settings (see Fig. 14) also applies for high weld settings of all the materials. Under high weld settings the consequence is bigger than above, and reasonable simulation is not possible. The elements encounter too heavy mesh distortion because they cannot gradually adapt to the geometrical changes, resulting in excess of heat generation and softening to a degree that the applied force cannot be withstand.

A numerical experiment is presented in the following to support the above discussion. It is emphasized that this is not prediction of the welding case, but only for discussion. The numerical experiment is based on cross-wire welding of stainless steel with a welding current of 12 kA during 600 ms weld time with an electrode force of 10 kN (the case corresponds to the above weld C). The mechanical material properties of the stainless steel are limited to remain constant after 1170 °C, such that the material has enough strength to withstand the electrode force without the need to deform heavily. After one third of the welding time (200 ms), the geometry and developed temperature field looks like depicted in Fig. 17a. It is naturally unrealistic because the molten ball would collapse if not kept artificially stiff, but a gradual collapse would not be possible to simulate due to the above discussion. Further 25 ms simulation leads to Fig. 17b. If instead, the realistic material properties are assumed to apply after Fig. 17a, a constant velocity of 50 mm/s produce the geometry depicted in Fig. 17c after 25 ms.

By doing this, a geometry (Fig. 17c) similar to the real geometry after welding with high current settings is obtainable, although after reaching an artificially high temperature. This cannot be used for prediction, but it proves that the deformation pattern including the contact between the two objects is potentially simulated as long as the softened volume is discretized by a sufficient number of elements.

Fig. 18 provides additional views of the geometry obtained in Fig. 17c for showing the similarity to the real case.

5. Summary

Cross-wire welding of stainless steel, structural steel and aluminum has been presented by experiments with focus on setdown, local interface properties and phase transformations in the structural steel. Numerical simulations are compared to the experiments and used to support the discussions. A number of conclusions can be drawn:

- The selection of the type of welding machine is crucial for successful welding. Proper follow up of the electrode force and movement is necessary, and the welding current should preferable be DC to avoid the high peaks necessary in AC to supply the same amount of energy. This is especially important for welding of aluminum wires requiring high welding current and short welding time.
- The electrical contact resistance is normally more important in spot welding, while the geometry is more important in projection welding. It was however found that the surface conditions are important in cross-wire welding, both to avoid splash and for getting consistent welds.

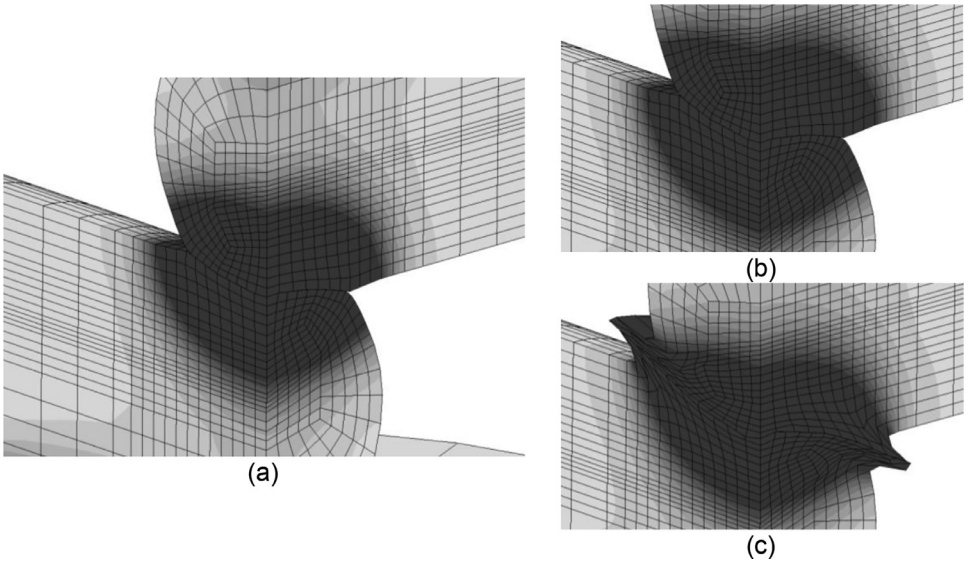

Fig. 17. Numerical experiment with material and weld settings corresponding to weld C (Fig. 6a and Fig. 7c) consisting of two stainless steel rods welded at high weld settings. The darkest color identifies melting. (a) Simulated 200 ms of the weld time with artificially stiff material at high temperatures. (b) 25 ms continuation from (a). (c) 25 ms continuation from (a) with material properties reflecting the actual temperatures, i.e. with softer material.

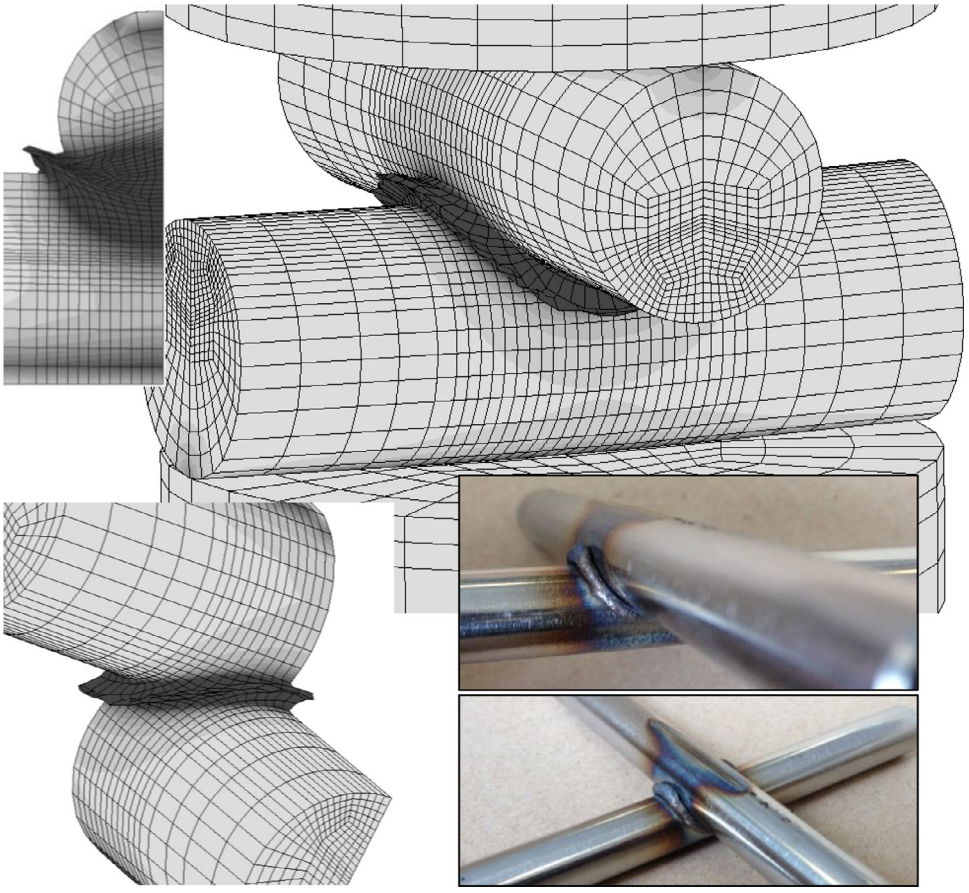

Fig. 18. Additional views of the numerical experiment corresponding to Fig. 17c. Two photos of the real weld are included.

- The development of flash when welding stainless steel or structural steel is different, and an analogy to friction welding was made. This also supports the conclusion that the welds are closer to solid state joining with only local melting than to a typical fusion weld.
- The simulations were able to match the experiments at low weld settings in terms of setdown and for the structural steel also in terms of simulated isothermal lines compared to phase transformations visible in the experimental cross-sections.
- Remaining challenges in simulation of high weld settings and flash generation are mainly remeshing and the ability to keep mesh refinement during remeshing. Another important aspect is the precise machine follow up of the electrode force and movement because slower follow up results in a larger volume of softened material to be squeezed out.

Declaration of Competing Interest

The authors declare that they have no known competing financial interests or personal relationships that could have appeared to influence the work reported in this paper.

Acknowledgments

Paulo Martins would like to acknowledge the support provided by Fundação para a Ciência e a Tecnologia of Portugal and IDMEC under LAETA-UIDB/50022/2020.

References

Batten, GH, 1958. Some aspects of cross wire welding of aluminium alloys. Br. Weld. J. 5 (9), 417–420.
Bushell, R, 1951. Resistance welding of cross-wire joints. Weld. Metal Fabr. 19 (5), 175–178.
Fukumoto, S, Morikawa, S, Yamamoto, A, 2008. Small-scale resistance welding of crossed tini fine wire. Mater. Sci. Forum 580-582, 225–228.
Fukumoto, S, Tsubakino, H, Zhou, Y, 2006. Heat input and deformation control in resistance microwelding of fine nickel wires. Weld. Int. 20 (9), 692–697.
Goodman, IS, 1950. Variables in cross-wire welding of dissimilar metals. Weld. J. 29 (10), 863–875.
Iatcheva, I, Darzhanova, D, Manilova, M, 2018. Modeling of electric and heat processes in spot resistance welding of cross-wire steel bars. Open Phys. 16 (1). doi:10.1515/phys-2018-0001.
Jones, RC, 1948. Resistance welding crossed wires. Weld. J. 27 (12), 703–714.
Jordan, RH, 1964. Productivity in multiple cross-wire welding. Weld. Metal Fabr. 32 (1), 19–26.
Khan, MI, Kim, JM, Kuntz, ML, Zhou, Y, 2009. Bonding mechanisms in resistance microwelding of 316 low-carbon vacuum melted stainless steel wires. Metall. Mater. Trans. A 40A, 910–919.
Knowlson, PM, 1967. Welding in electronics. Br. Weld. J. 14 (7), 398–400.
Mikno, Z, 2018. Cross-wire projection welding of aluminium alloys in relation to pneumatic and electromechanical electrode force systems. Therm. Sci. Eng. 1. doi:10.24294/tse.v1i4.515.
Nielsen, C, Martins, P, Zhang, W, Bay, N, 2011. Mechanical contact experiments and simulations. In: Proceedings of the 10th International Conference on Technology of Plasticity, In: Steel Research International, 82, pp. 645–650.
Nielsen, CV, 2012. 3D Modeling and Testing of Contact Problems in Resistance Welding PhD Thesis. Technical University of Denmark.
Nielsen, CV, Fernandes, JLM, Martins, PAF, 2013. All-hexahedral meshing and remeshing for multi-object manufacturing applications. Comput. Aided Des. 45, 911–922.
Nielsen, CV, Zhang, W, Alves, LM, Bay, N, Martins, PAF, 2013. Coupled Finite Element Flow Formulation In: Modelling of Thermo-Electro-Mechanical Manufacturing Processes with Applications in Metal Forming and Resistance Welding. Springer-Verlag, London, UK. doi:10.1007/978-1-4471-4643-8_3.
Nielsen, CV, Zhang, W, Martins, PAF, Bay, N, 2015. 3D numerical simulation of projection welding of square nuts to sheets. J. Mater. Process. Technol. 215, 171–180.

Nielsen, CV, Zhang, W, Perret, W, Martins, PAF, Bay, N, 2015. Three-dimensional simulations of resistance spot welding. Proc. Inst. Mech. Eng. Part D: J. Autom. Eng. 229 (7), 885–897.
Pan, R, Watt, DF, 1995. Simulating microstructure development in high-carbon steel cross-wire welding. Weld. J. 74 (12), 385s–395s.
Resistance Welding Manufacturers' Association, 2003. Resistance welding manual. RWMA, Philadelphia.
Scotchmer, N, 2007. The other resistance process: Cross wire welding. Weld. J. 86 (12), 36–39.
SORPAS® 3D.welding. SWANTEC Software and Engineering. 2020 Available at https://www.swantec.com/products/sorpas-3d/
Thornton, PH, Krause, AR, Davies, RG, 1996. Contact resistances in spot welding. Weld. J. 75 (12), 402s–412s.
Wängsjö, H, Palmqvist, A, 1958. The resistance welding of crossed wires. ASEA J. 31 (3), 27–36.